# Cyclic-loading-induced Accumulation of Geometrically Necessary Dislocations Near Grain Boundaries in an Ni-based Superalloy

**E-Wen Huang, Rozaliya I. Barabash, Gene E. Ice, Wenjun Liu, Yee-Lang Liu, Ji-Jung Kai, and Peter K. Liaw**

*In this study, the fatigue-induced microstructure produced in a nickel-based polycrystalline superalloy that was subjected to cyclic loading was characterized by polychromatic x-ray microdiffraction (PXM) together with in-situ neutron diffraction and transmission-electron microscopy (TEM). In-situ neutron-diffraction measurements reveal two distinct stages of the fatigue damage: cyclic hardening followed by cyclic softening. Three-dimensional spatially resolved PXM micro-Laue measurements find an increase in the density of geometrically necessary dislocations near the grain boundaries, which is accompanied by lattice rotations and grain subdivisions. The PXM results are in agreement with the in-situ neutron-diffraction and TEM results.*

## INTRODUCTION

Superalloys are a group of nickel- and cobalt-based materials that show exceptional strengths for high-temperature applications. These materials are optimized for use in aircraft engines, turbine blades, and other high-temperature applications.[1] Typically, precipitate-strengthened nickel-based superalloys have higher strength than cobalt-based superalloys.[2] The precipitate-strengthened nickel-based superalloys are widely used in the chemical and aircraft industry, especially in cyclic-loading environments, such as in pistons, turbines, and engines.

Because of the continuous nature of cyclic loading, metal fatigue is one of the most important damage mechanisms that promotes premature failure. Research on fatigue damage is of great interest to both the industrial and the fundamental research communities because of its practical importance and because it underpins the structural evolution of many mechanical materials.[3] A critical first step toward understanding fatigue mechanisms is to characterize how different microstructures respond to cyclic deformation.

Recently, Gopinath et al.[4] reported on the low-cycle-fatigue behavior of a precipitate-strengthened nickel-based superalloy. Their transmission-electron microscopy (TEM) studies revealed that, in addition to precipitate shearing, dislocation activity of the matrix plays an important role in fatigue damage. During fatigue, polycrystalline grains may deteriorate into deformation structures with different crystallographic orientations on a micrometer scale.[5] As mentioned in Mughrabi's latest review article,[3] ". . . Today, it is clear that mechanisms of cyclic microplasticity, based on the glide of dislocations, are responsible for the fatigue phenomena . . . ".

In this study, we investigate cyclic-loading-induced microplasticity in a nickel-based superalloy, resulting in fatigue failure. Our focus is on the accumulation of geometrically necessary dislocations (GNDs) near the deformation-induced grain boundaries. The current approach benefits from the recent development of three-dimensional (3-D) polychromatic x-ray microdiffraction (PXM). Polychromatic x-ray microdiffraction has the unique ability to nondestructively characterize near and sub-surface crystal structures of defects with

### How would you...

**...describe the overall significance of this paper?**

*Metal fatigue is one of the most important damage mechanisms which promotes premature failure. This paper provides new insight into the microstructure, subjected to fatigue damage, by combining the ensemble-average neutron and the spatially resolved synchrotron x-ray microbeam results. Understanding microplastic deformation mechanisms during cyclic loading allows for the development of new nickel-based superalloys.*

**...describe this work to a materials science and engineering professional with no experience in your technical specialty?**

*Research on fatigue damage is of great interest to both the industrial and the fundamental research communities because it underpins the structural evolution of many mechanical materials. This paper examines the effects of the cyclic deformation on a nano-precipitate strengthened alloy. In-situ diffraction experiments reveal that cyclic hardening/softening phenomena take place during fatigue of the nickel-based superalloy. The synchrotron x-ray microbeam results expose the spatially resolved grain-subdivision structure and cumulative local texture induced by cyclic loading at the micro-scale.*

**...describe this work to a layperson?**

*Superalloys, which are widely applied in the aircraft, chemical, and transportation industry, require better understanding of their fatigue properties. This work is intended to study the fatigue damage on the superalloys. This work has identified several deformation mechanisms evolving in the superalloy during fatigue at different structural levels.*

submicrometer three-dimensional (3-D) resolution. More specifically, the depth-resolved technique allows for investigation of the depth-dependent strain and dislocation gradients on the micro-scale.[6–10]

In addition to local strain and dislocation mapping with PXM at the microscale, neutron-diffraction experiments were performed to obtain the ensemble-averaged structural information during fatigue experiments.[11–13] The in-situ neutron-diffraction measurements at the ISIS spallation source in the Rutherford Appleton Laboratory, United Kingdom, make it possible to monitor microstructural-parameter evolution of both the matrix and the precipitates, and connect with the bulk properties and the lattice-strain evolution during cyclic loading.

The combination of these two novel techniques, together with TEM analysis, provides for unique information

## EXPERIMENTAL PROCEDURES

### Material

An aged nickel-based superalloy (Ni-21Cr-17Mo in weight percentage) was used with an average grain size ≈70 μm. The alloy contains about a 25% volume of nano-precipitates. These $Ni_2$(Cr,Mo)-phase nano-precipitates are embedded in the face-centered-cubic (f.c.c.) matrix. Transmission electron microscopy (TEM)[14] and small-angle neutron scattering (SANS)[15] experiments found the ellipsoidal precipitates to be about 12 nm in diameter. The aged alloy was machined into a dog-bone shape for in-situ neutron-diffraction measurements, as shown in Figure Aa.

### Low-cycle-fatigue Experiments and in-situ Neutron-diffraction

A gauge volume of ≈60 $mm^3$ near the center of the specimen was used through the low-cycle-fatigue experiments. The tests were carried out with the stress-rig at ENGIN-X, the ISIS spallation source in the Rutherford Appleton Laboratory, U.K.[16] Time-of-flight diffraction patterns were acquired with data collection times of 40 minutes, during straining for statistically sufficient diffracted intensity. The Rietveld method was applied to fit the diffraction patterns. The neutron-diffraction profiles were refined by the General Structure Analysis System (GSAS).[17,18] The low-cycle-fatigue (LCF) experiments were conducted under fully reversed (R = –1) loading conditions with a strain range ±1%. The cyclic frequency was 0.5 Hz. The neutron-diffraction data were collected after different numbers of cycles during the fatigue experiments: N = 1, 4, 8, 30, 100, 250, 500, and 1,000.

### Transmission-electron Microscopy

Specimens for LCF experiments had a dog-bone shape. For TEM studies thin slices with a diameter of 3 mm and thickness of approximately 0.3 mm were cut from the center of the specimens before and after cyclic loadings, as shown in Figure Aa. These slices were further ground to a thickness of about 0.1 mm. Electron-transparent thin foils were prepared by the twin-jet electropolishing technique (temperature = 15°C, voltage = 25 V, and current = 0.6 A), employing a solution containing 640 mL orthophosphoric acid, 150 mL concentrated sulfuric acid, 35 mL concentrated hydrochloric acid, and 210 mL distilled water. The foils were examined by TEM at an operating voltage of 200 kV, utilizing the bright-field (BF) mode.

### Synchrotron X-ray Microbeam Experiments

In addition to the ensemble-average neutron experiments, we employed polychromatic three-dimensional (3-D) x-ray microdiffraction (PXM) to study local structural evolution. An incident beam with the energy range of 5–25 keV was used to produce Laue patterns from the subgrain volumes probed by the incident beam. Experiments were made on station 34-ID-E at the Argonne National Laboratory Advanced Photon Source, which is the world's first 3-D polychromatic x-ray microprobe. This station has point-to-point sub-micrometer spatial resolution using the differential-aperture depth profiling and the depth-resolved analysis technique.[8,9,19] The primary advantage of PXM is the ability to determine crystalline structure without sample rotations. Polychromatic x-ray microprobe using high-energy x-rays facilitates the investigation of the individual grains embedded in a polycrystal with sub-micrometer spatial resolution below the surface of bulk samples. With the advantages of the PXM, the local phase of crystalline materials, the local orientation and, therefore, the grain and phase boundary structures, the local defect distributions, including elastic and plastic strains, were studied for the nickel-based superalloy after cyclic loading. Two samples were prepared. Sample 1 was the reference sample (before cyclic loading) and Sample 2 was after N = 250, which was within the cyclic-softening stage. The PXM geometry and relative orientation of the sample to the beam are shown in Figure Ab.

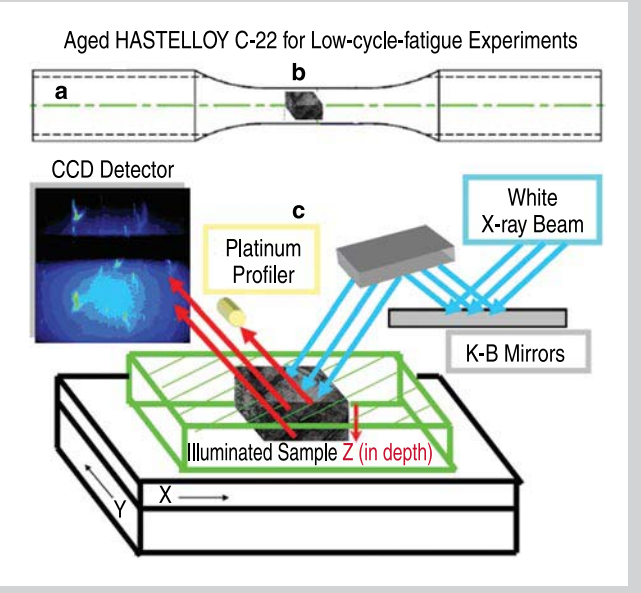


Figure A. (a) Specimen geometry for the low-cycle-fatigue experiments. (b) PXM specimen prepared in the middle of the specimen. (c) Geometry of the PXM measurements: a white x-ray microbeam collimated by K-B mirrors illuminates a deformed specimen on a sample holder. The holder can move along three axes to collect the three-dimensional information. The diffraction from the sample is registered on a CCD area detector. A Pt wire profiler is controlled with a submicrometer step to resolve the origin of the diffraction along the incident beam.

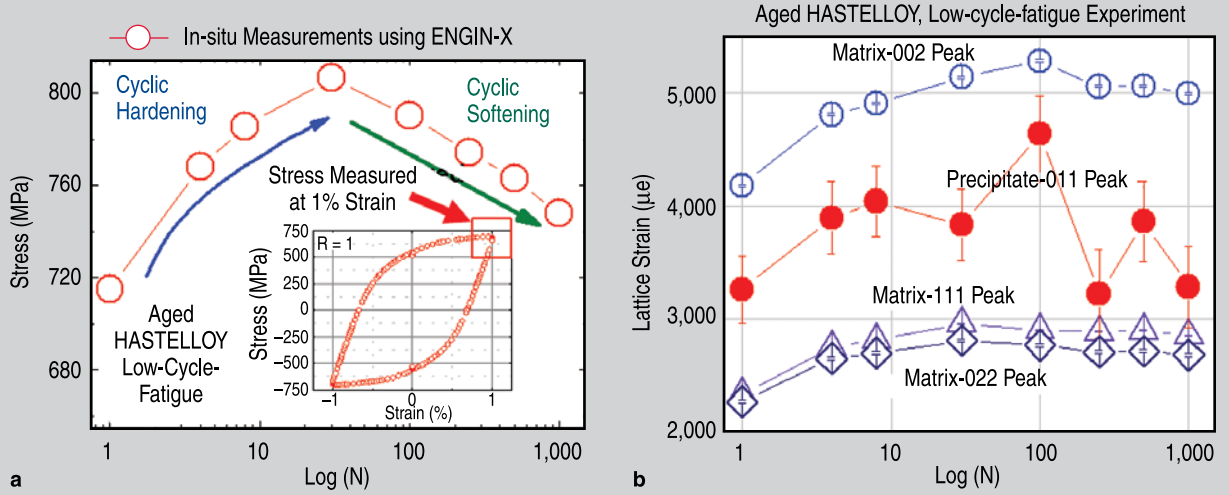


Figure 1. Low-cycle-fatigue data measured at 1% tensile strain: (a) the stress-evolution shows the cyclic hardening and softening. (b) The lattice-strain evolution as a function of fatigue cycles along the following local crystallographic directions in the matrix: [022] (diamonds), [111] (triangles), and [002] (open circles). The lattice strain of the nano-precipitate along [011] direction (filled red circles). The inset in (a) illustrates a stress-strain loop during one complete fatigue cycle. The red square is marked to indicate that for each cycle the stress was measured at 1% tensile strain.

about the fatigue-induced microstructure evolution at the microscopic and macroscopic scales. See the sidebar for experimental procedures.

## RESULTS AND DISCUSSION

### Volume-averaged Anisotropic Lattice Strains

A statistical understanding of the microstructure evolution during fatigue loading was advanced by in-situ neutron-diffraction experiments, which eliminate the differences due to sample preparations. In-situ neutron-diffraction measurements during the LCF experiments study the bulk-average-property and the lattice-stain evolution as a function of the fatigue cycles. The macroscopic tensile stresses at 1% strain are presented in Figure 1a as a function of N. The neutron experiments conducted at 1% strain of the fatigue cycles are present in terms of the lattice-strain (d-spacing) development along several crystallographic directions in the matrix and nano-precipitates (Figure 1b). At each fatigue cycle, the measurements were performed at 1% tensile strain. The location of this point at the stress-strain loop, during one complete fatigue cycle, is marked with a red square in the inset of Figure 1a. The lattice strain and stress values in Figure 1 correspond to the macroscopic 1% tensile strain, which is why lattice strain along all crystallographic directions demonstrates the extension. The lattice parameter $a_0$ of the alloys before the cyclic loading was determined by neutron diffraction to equal 0.3605 nm, which is further used to index the PXM results. The peak-stress ($\sigma_{max}$) values during these experiments were below 815 MPa, which is greater than the 0.2% yield stress of the alloy. The bulk-averaged strain-stress evolution (Figure 1a) shows that there are two stages along the cyclic loading in the alloy: cyclic hardening in the first 30 cycles and then cyclic softening. Similar cyclic hardening/softening phenomenon was also observed in the other precipitate-strengthened nickel-based alloys at room temperature.[4]

Anisotropic and non-monotonic lattice-strain evolution is revealed (Fig-

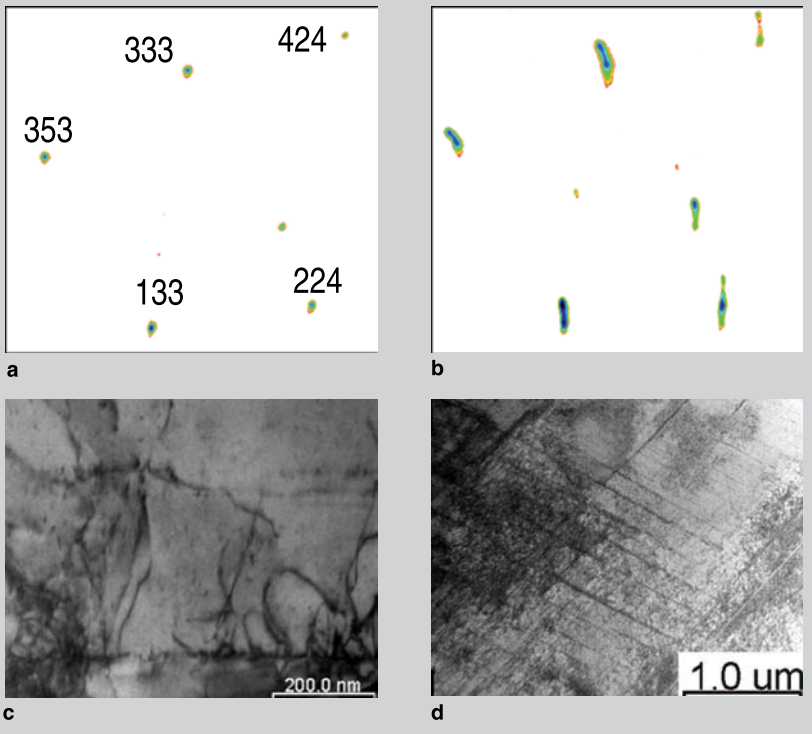


Figure 2. Laue patterns (a) before and (b) after cyclic deformation; (c) and (d) are TEM images.

ure 1b) by neutron-diffraction-profile analysis. Lattice strains of both the matrix and the precipitates grow along all crystallographic directions during the cyclic hardening up to N= 30. The onset of cyclic softening typically occurs after N=30, after which the volume-averaged lattice strain in the matrix saturates and slightly decreases. Moreover, the lattice strain of the nanoparticles along the [011] direction also decreases. The cyclic hardening and softening behavior has been revealed from the microstructure evolution.[4,5,11,12] The generation of the dislocations is responsible for the cyclic hardening. The annihilation and the rearrangement of the dislocations contribute to the cyclic softening.[5,11,12]

With these results, the question now becomes "how can we quantify the local spatially varying microstructure after cyclic loading at the microscale?" During deformation of the multicomponent systems, local stresses change significantly since the deformation is markedly inhomogeneous. However, force balancing requires that the volume averaged stress within the sample must equal the external applied stress.

Thus, while some components may exhibit significant compressive stresses, others must exhibit competing tensile stresses. This may cause the formation of large strain gradients at the microscale. To understand the anisotropic evolution of the inhomogeneous internal-strain fields and their correlations with the development of the cumulative dislocation sub-structure at the micro-scale, and to study the detailed spatially-resolved microstructure and the local texture, the materials are further explored via PXM in the beginning of LCF and within the cyclic-softening stage.

## Inhomogeneous Distributions of Internal Strains and Geometrically Necessary Dislocations

Distinct inhomogeneous dislocations distributions are formed during (cyclic) plastic deformation.[3,10,20] The PXM method is well suited for submicrometer analysis of such inhomogeneous deformation-induced structures. Laue patterns from undeformed crystal grains contain sharp Laue spots. The formation of the statistically stored dislocations (SSD), GNDs, and geometrically necessary boundaries (GNBs) causes both local-strain fluctuations and strongly correlated long-range mesoscopic rotations within grains or subgrains.[6,21,22] Such correlated deformation spreads the conditions for x-ray scattering in reciprocal space near each (*hkl*) lattice-plane normal and causes streaking of the Laue spot. When GNDs form, each (*hkl*) Laue spot is strongly elongated (streaked) in a specific direction, depending on the mutual orientation between the GNDs slip system and the direction of the incident beam. The details of the streaked Laue patterns analysis can be found elsewhere.[6,21,22] When the orientation of the lattice changes with depth, different layers scatter x-rays incoherently, thus differential aperture x-ray microscopy (DAXM) can be applied to characterize depth-dependent orientation changes.[8,9]

**Thus, while some components may exhibit significant compressive stresses, others must exhibit competing tensile stresses.**

Typical Laue patterns before and after the cyclic loading are shown in Figure 2a and b, respectively. Before the cyclic loading, the relatively sharp and round diffraction spots corresponding to a perfect crystal are seen (Figure 2a). The elongated streaks in Figure 2b indicate the formation of GNDs dislocation populations after cyclic loading.

The plastic responses of the material in the grain can be described by the formation of the patterned cell-block dislocation structure in the material to relax the stress field induced from the cyclic loadings. The formation of the patterned-dislocation cell-block structure is also seen from TEM (Figure 2d). In contrast, before deformation, TEM shows only low-density randomly distributed SSDs. On the other hand, TEM shows that fatigue induces a significant increase of the dislocation density, causes grain subdivision, and the formation of the patterned-dislocation structures. Subgrain boundaries are distinguished in the TEM observations. This agrees with Gopinath et al.'s observation[4] that during cyclic loading, the grains have split into differently oriented fragments (subgrains) due to subdivision.[23]

To further study the different types of the microstructures, PXM was applied with the 3-D depth-resolved DAXM technique to follow the accumulation of the lattice rotation, GNDs, GNBs, and grain subdivision as a function of the depth. This allows for characterization of the defect distribution near boundaries and near the fracture surface. The indexed Laue patterns were analyzed at different depths to investigate the local texture and strain gradients distribution.

## Real-space Orientation Maps and Pole Figures

With PXM, automated indexing is performed by comparing the pattern of angular differences between reflections corresponding to different possible crystal orientations. Typically, at least ten Laue spots with different (*hkl*)s are compared until a match is found.[24] For example, Figure 2a shows the indexed peaks of a face-centered-cubic (f.c.c.) structure. The local crystallographic texture in the polycrystalline specimens is, then, determined, based on the local orientation.

The lattice parameter used for indexing, 0.3605 nm, was taken from the neutron diffraction results. As a result of many indexations[24] a real-space orientation map of the specimen is reconstructed over a larger area (Figure 3). The reconstructed pole figure is shown in Figure 3a. The pole figure offers information about the sample orientation distribution function with high resolution on local orientations. The locations of the (001), (100), and (010) poles are identified (Figure 3a). The measured orientation distributions around these three poles are magnified

to reveal the local-strain distribution at higher resolution (Figure 3c, d, and e). The orientation distributions around these three poles are practically orthogonal to each other. Orientation fluctuations around all three poles are within the range of 0.4–0.75 degrees.

The presence of a GNB is indicated by two groups of the diffraction spots with an abrupt orientation change (marked with green in Figure 3a) indicating the existence of a GNB embedded beneath the sample surface.

Three-dimensional depth-resolved measurements were performed in locations containing at least two grain subdivisions using a knife-edge-type differential aperture. It is then possible to reconstruct the lattice rotation along the beam as it penetrates into the sample, and to reveal the distribution of GNDs and GNBs within the grain subdivisions (Figure 3b). The orientation differences at very large distances are shown in the reconstructed real-space maps (Figure 3b). Such orientation differences in different sub-grains could possibly result from stress incompatibilities at the grain boundaries caused by the grain-grain interactions under cyclic loading. The existence of these orientation differences over large distances is in agreement with the low-energy-dislocation-structure (LEDS) principle. Thus, alternating point-to-point misorientations are suppressed by a gradient towards another orientation.[25]

### Angle Rotation as a Function of Depth Revealing the GNBs

Using the high-spatial resolution of the PXM (≈0.5 μm), the two grain subdivisions were investigated in detail as shown in Figure 4. A schematic depth-resolved scan is shown in Figure 4a. Indexed Laue patterns corresponding to different depths under the sample surface are presented in Figure 4b, c, d. Near the surface, the lattice orientation (grain subdivision 1) is close to a 333 normal. At a depth of 10 μm, the diffraction from both subdivisions 1 and 2 are observed simultaneously (Figure 4c and f). The second group of the diffraction spots corresponding to the deeper subgrain lattice orientation is marked in purple. The diffraction spots resulting from the near-surface subgrain vanish between 15 μm and 30 μm below the surface.

An important result from the depth-resolved grain subdivision study was the characterization of the orientation distribution at and near a grain boundary. The depth-dependent orientation distribution function (Figure 5) shows lattice rotations as a function of depth. The change of the lattice orientation as a function of the distance from the sample surface and from the near-surface boundary (highlighted by a blue arrow) finds that the lattice-orientation rotates gradually in the sub-grain near the surface (subdivision 1). However, the orientation is almost constant in the embedded sub-grain (subdivision 2), which lies beneath the surface. The inset pole figure depicts two groups of indexed orientations from subdivisions 1 and 2, respectively. There is an abrupt rotation of ≈4° between the subgrains.

**A distribution of geometrically necessary dislocations is strongly influenced by the geometrical constraints from the surrounding grains, distance to the free surface and boundaries, and by the grain orientation.**

The different character of lattice rotations near the boundary observed in the two subgrains probably arises from the differences in their geometrical constraints and from their slightly different orientations. The number of constraints increases as a function of the depth away from the surface. The observed depth-dependent gradient results in cumulative rotations and formation of GNDs, and occupies regions within the length-scale about 10–30 μm. Lattice rotations and grain subdivisions are also evidence of cyclic-loading damage. They indicate the evolution of a hierarchical dislocation-based mesoscopic substructure, evolving as a result of the translational-rotational movement of the grain with the free surface during the cyclic loading due to both shear and rotation.

## CONCLUSIONS

Volume-average in-situ neutron experiments demonstrate that cyclic hardening/softening phenomena take place as a function of fatigue cycles during LCF of the nickel-based superalloy. The generation of the dislocations is responsible for the cyclic hardening. The annihilation and the rearrangement of the dislocations contribute to the cyclic softening.

High-spatial resolution synchrotron x-ray microbeam experiments were applied to characterize the inhomogeneities of the cyclic-loading-induced microstructure evolution near the grain boundaries of the nickel-based polycrystalline superalloy. The spatially resolved microstructure demonstrates the formation of the cumulative local texture induced by cyclic loading at the micro-scale. Cyclic-deformation-induced geometrically necessary dislocations and boundaries were found. A distribution of geometrically necessary dislocations is strongly influenced by the geometrical constraints from the surrounding grains, distance to the free surface and boundaries, and by the grain orientation. The PXM findings correlate with the TEM and neutron diffraction results.

## ACKNOWLEDGEMENTS

*This research is supported by the National Science Foundation (NSF), International Materials Institutes (IMI) Program (DMR-0231320). E-W. H. gratefully acknowledges the Ludo Frevel Crystallography Scholarship from The International Centre for Diffraction Data (ICDD). We greatly appreciate the neutron beam time from the ENGIN-X of the Rutherford Appleton Laboratory, United Kingdom (proposal number: RB720509). R.I.B. and G.E.I. are sponsored by the Division of Materials Science and Engineering, Office of Basic Energy Science, U.S. Department of Energy. W.L. and*

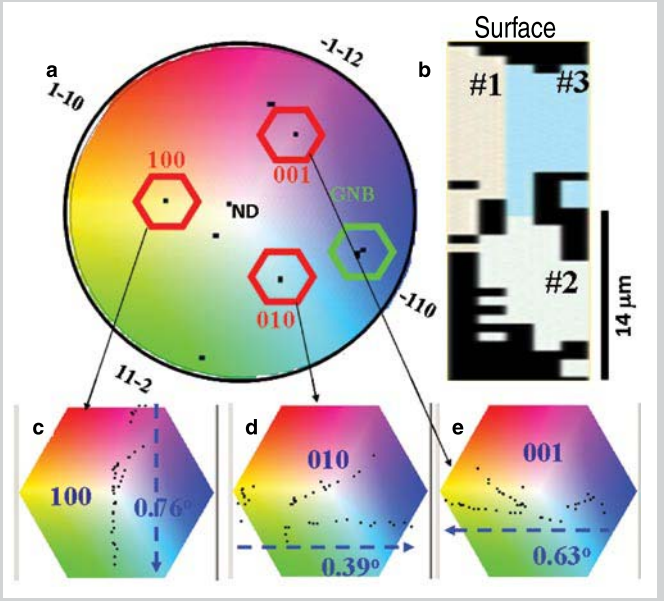


Figure 3. (a) A reconstructed pole figure with the (001), (010) and (100) poles; (b) the reconstructed real space map showing the locations of the three probed grains; (c), (d), (e) enlarged regions of the pole figure showing the orientation distribution around the 001, 100, 010 poles.

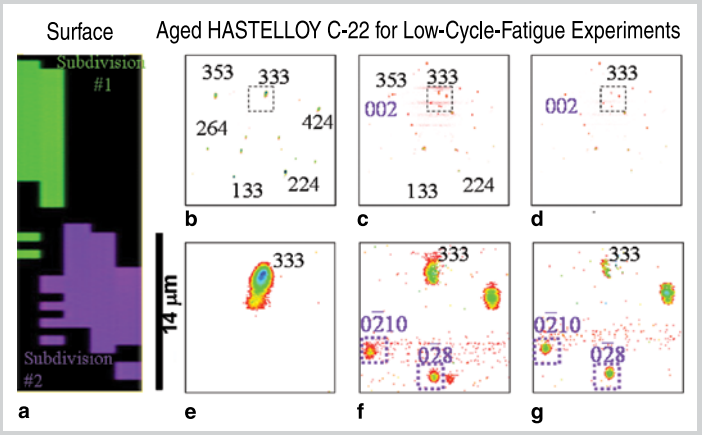


Figure 4. (a) Reconstructed real space map showing location of the GNB corresponding to Figure 3a. Laue patterns from (b) grain subdivision 2, (c) boundary region between subdivisions 1 and 2, and (d) subdivision 2; enlarged regions around the centers of the Laue patterns are shown in (e), (f), (g), respectively.

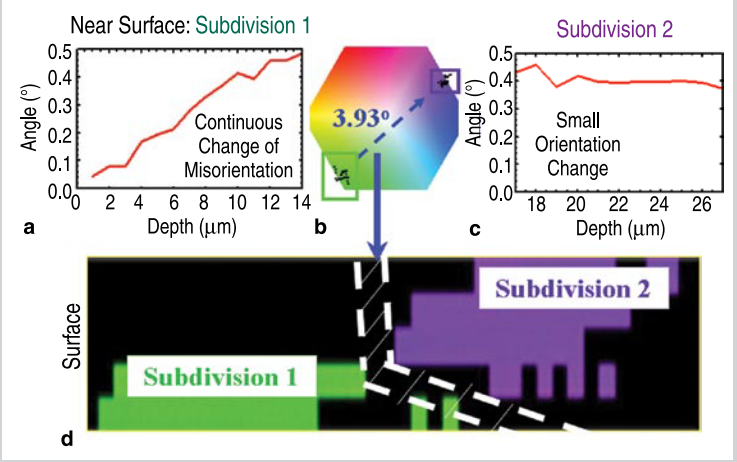


Figure 5. (a) Depth-dependent lattice rotations in subdivisions 1 and 2. (b) The reconstructed pole figure from the boundary region. (c) Depth-dependent angle evolution in subdivision 2. (d) The reconstructed real space map of the two subdivisions.

*the use of the Advanced Photon Source are supported by the U.S. Department of Energy, Office of Science, and Office of Basic Energy Science. We gratefully acknowledge L. Levine and M. Stoudt for most valuable comments and suggestions.*

## References

1. G.L. Erickson, *ASM Handbook*, 10th edition, 1 (1990), pp. 981–994.
2. J. Sato et al., *Science*, 312 (2006), pp. 90–91.
3. H. Mughrabi, *Metallurgical and Materials Transactions A*, 40 (2009), pp. 1257–1279.
4. K. Gopinath et al., *Acta Materialia*, 57 (2009), pp. 3450–3459.
5. B. Bay et al., *Acta Metall. Mater.,* 40 (1992), pp. 205–219.
6. R.I. Barabash et al., *Appl. Phys. Letters*, 79 (2001), pp. 749–751.
7. R.I. Barabash et al., *Micron*, 40 (2009), pp. 28–36.
8. B.C. Larson et al., *Nature,* 415 (2002), pp. 887–890.
9. B.C. Larson et al., *J. of Engineering Mat. and Technol.,* 130 (2008), 0210241.
10. L.E. Levine et al., *Nature Materials*, 5 (2006), pp. 619–622.
11. E-W. Huang et al., *International J. of Fatigue*, 29 (2007), pp. 1812–1819.
12. E-W. Huang et al., *International J. of Plasticity*, 24 (2008), pp. 1440–1456.
13. E-W. Huang et al., *Met. Mat. Trans. A*, 39 (2008), pp. 3079–3088.
14. Y.L. Lu et al., *Scripta Materialia*, 56 (2007), pp. 121–124.
15. E-W. Huang et al., *Appl. Phys. Lett.,* 93 (2008), 161904.
16. J.R. Santisteban et al., *J. Appl. Cryst.,* 39 (2006), pp. 812–825.
17. A.C. Larson and R.B. Von Dreele, *General Structure Analysis System* (Los Alamos National Laboratory Report LAUR 86-748 [2004]), pp. 160–165.
18. R.B. Von Dreele, J.D. Jorgensen, and C.G. Windsor, *J. of Appl. Cryst.*, 15 (1982), pp. 581–589.
19. H. Bei et al., *Appl. Phys. Lett.*, 93 (2008), 071904.
20. H.F. Poulsen, U. Lienert, and W. Pantleon, *Mat. Sci. Technol.*, 21 (2005), pp. 1397–1400.
21. G.E. Ice and R.I. Barabash, *Dislocations in Solids*, Vol.13, ed. F.R.N. Nabarro and J.P. Hirth (Maryland Heights, MO: Elsevier, 2007), pp. 500–601.
22. R.I. Barabash et al., *J. Appl. Phys.*, 93 (2003), pp. 1457–1464.
23. Q. Liu, D. Juul Jensen, and N. Hansen, *Acta Mater.*, 46 (1998), pp. 5819–5828.
24. J.S. Chung and G.E. Ice. *J. Appl. Phys.,* 86 (1999), pp. 5249–5255.
25. D. Kuhlmann-Wilsdorf, *Scr. Metall. Mater*, 27 (1992), pp. 951–956.

**E-Wen Huang, graduate research assistant, and Peter K. Liaw, Professor and Ivan Racheff Chair of Excellence, are with the Department of Materials Science and Engineering, University of Tennessee, Knoxville, TN; Rozaliya I. Barabash, research professor, and Gene E. Ice, corporate fellow, are with the Materials Science and Technology Division, Oak Ridge National Laboratory, Oak Ridge, TN; Wenjun Liu, assistant physicist, is with Advanced Photon Source, Argonne National Laboratory, Argonne, IL; Yee-Lang Liu, currently serving in the army, and Ji-Jung Kai, professor, are with the Department of Engineering and System Science, National Tsing-Hua University, Hsinchu, Taiwan. Prof. Barabash can be reached at (865) 241-7230; e-mail barabashr@ornl.gov.**